DESIGN AND VALIDATION OF ROBUST AND AUTONOMOUS CONTROL FOR NUCLEAR REACTORS

ROMAN A. SHAFFER†, ROBERT M. EDWARDS**, and KWANG Y. LEE* (corresponding author)
†The US Nuclear Regulatory Commission
Rockville, MD, USA
E-mail : ras3@nrc.gov
**Department of Mechanical and Nuclear Engineering
*Department of Electrical Engineering
The Pennsylvania State University
University Park, PA USA
E-mail : rmenuc@engr.psu.edu, kwanglee@psu.edu

Received February 8, 2005

A robust control design procedure for a nuclear reactor has been developed and experimentally validated on the Penn State TRIGA research reactor. The utilization of the robust controller as a component of an autonomous control system is also demonstrated. Two methods of specifying a low order (fourth-order) nominal-plant model for a robust control design were evaluated: 1) by approximation based on the "physics" of the process and 2) by an optimal Hankel approximation of a higher order plant model. The uncertainty between the nominal plant models and the higher order plant model is supplied as a specification to the μ-synthesis robust control design procedure. Two methods of quantifying uncertainty were evaluated: 1) a combination of additive and multiplicative uncertainty and 2) multiplicative uncertainty alone. The conclusions are that the optimal Hankel approximation and a combination of additive and multiplicative uncertainty are the best approach to design robust control for this application. The results from nonlinear simulation testing and the physical experiments are consistent and thus help to confirm the correctness of the robust control design procedures and conclusions.

KEYWORDS : robust control, autonomous control, reactor control, research reactor, experimental validation

1. INTRODUCTION

Low-level controllers designed with off-line and on-line robust control techniques have been studied as part of an intelligent control system with a high degree of autonomy for nuclear reactors [1]. This paper summarizes the framework of the low-level robust control design procedure and provides an assessment of alternative approaches in defining the nominal model and associated uncertainties. The assessment includes results from both nonlinear simulation testing and physical experiments conducted with the Penn State nuclear research reactor [2,3]. The remainder of this introduction provides background information to frame the robust control design and validation research.

1.1 History of Advanced Direct Control Experiments at the Breazeale Reactor

Much work has been done as part of the NSF/EPRI funded *Experimental Development of Power Reactor Intelligent* Control experiment [4]. Several major tasks were completed, including experimental validation and comparison of advanced direct control algorithms (optimal [5], robust [6], fuzzy logic [7], and neural networks [8]), and intelligent control research emphasizing a re-configurable supervisory control level to accommodate wide range operation and faulted conditions. An advanced degree was granted for work done by Walter [1] along these same lines. In Walter's work, he developed a system of execution-level robust controllers (over a wide power range of operation and rod velocity gain variation) and the necessary fuzzy-based supervisory level required for highly autonomous control. Though, he did not consider directly the highest-level coordination level in his work (see Figure 1).

1.2 High Autonomous Control Systems

An highly autonomous control system is a system with several levels of control, the top-most level being the least precise but most intelligent, and the lowest level

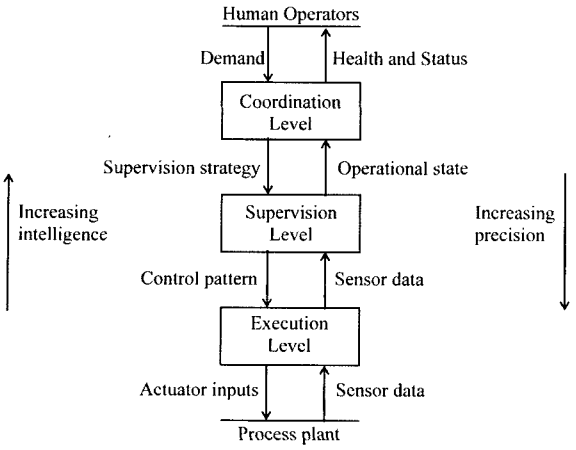

Fig. 1. Hierarchical Structure of a High Autonomy Control Architecture.

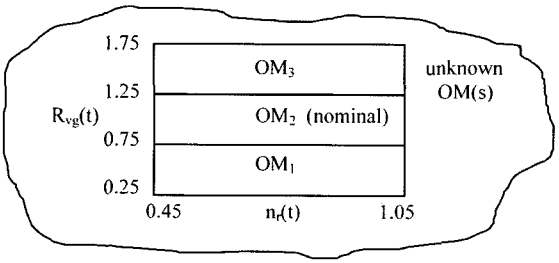

Fig. 2. Operational Modes.

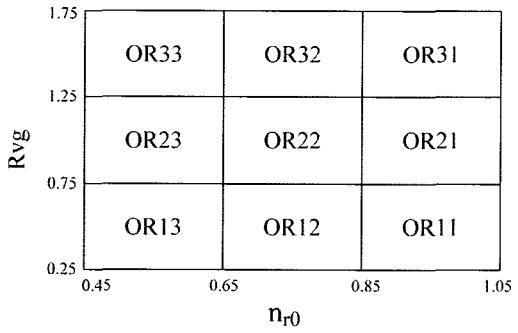

Fig. 3. Operational Regions for Robust Control Design.

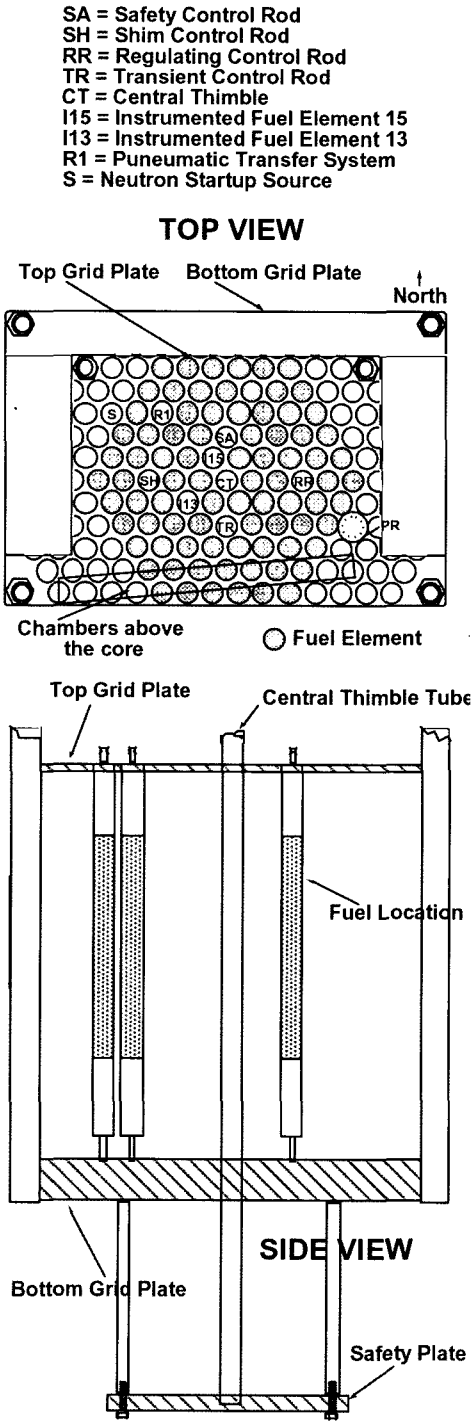

Fig. 4. Layout of the Penn State Breazeale TRIGA Reactor.

having the greatest precision but least intelligence, as pictured in Figure 1 [1]. These hierarchical levels can be defined spatially (according to the components of the physical system) or functionally (where a task is divided into sub-tasks), and most highly autonomous control systems will have elements of each to a certain degree. The level with greatest precision and least intelligence interfaces to the system's sensors and actuators and is referred to as the 'execution level.'

Functionally decomposing a two dimensional

operational space (depicted in Figure 2) into operational modes (OMs)—where the space outside these OMs is considered as an unknown OM (or OMs)—then OMs represent the different operating ranges of the variables belonging to the process plant in Figure 1. These variables are rod velocity gain (R_{vg}) and relative reactor power (n_r). The ranges could define a start up OM, a maneuvering OM, an on-line maintenance OM, or even a faulted OM. However, a single controller to accommodate the entire OM that also provides acceptable performance may be difficult to find. Therefore, the OMs are partitioned into operating regions (ORs)—Figure 3 [7,8].

Further, let OM_1 and OM_3 define OM_s representing rod reactivity changes due to rod actuator faults, and OM_2 the nominal OM, where OR_{21}, OR_{22}, and OR_{23} all belong to OM_2. Under this framework, the system uncertainty can be separated into parametric (structured) uncertainty and modeling (unstructured) uncertainty for robust control design of execution level controllers.

1.3 Reactor System Available for Control Experiments

The Penn State Breazeale Reactor (PSBR) is a General Atomic MARK III TRIGA (**T**raining, **R**esearch, **I**sotopes, **G**eneral **A**tomic). It is part of the Penn State Radiation Science and Engineering Center, RSEC, and is the longest operating university reactor in the United States. The reactor is a light-water cooled and reflected pool type reactor capable of routine pulse operation to 1000 Megawatts (MW) and constant power operation at 1 MW maximum. The reactor core has a basic shape of a right hexagonal prism containing about 100 fuel elements, Figure 4. There are 4 control rods designated as the safety rod, regulating rod, shim rod, and transient rod.

With periodic upgrades over its nearly 50-year lifetime, the facility has enabled the university to familiarize students with the current instrumentation technology that they would expect to find in industry. In 1991, the original analog-based control and monitoring system was replaced with a modern microprocessor-based system [9]. The reasons for this replacement are similar to the problems that face operators of existing U.S. nuclear power plants. Since the control systems for existing U.S. nuclear power plants were designed in the 60s and 70s, spare parts and technical assistance to maintain obsolete technology are becoming more difficult to secure. Modern digital control hardware and software can address the need to replace the obsolete technology and also provide more reliability and increased functionality to improve safety and performance.

1.4 Experimental Control Capacity

Check-out of the new digital system, prior to replacement of the analog control system, was accomplished with the aid of an experimental procedure created within the existing technical specifications of the TRIGA reactor [9]. The essential component of this procedure is a means for an experimental setup to change reactor power through an Experimental Changeable Reactivity Device (ECRD). An ECRD is implemented in the TRIGA reactor as a moveable absorber material within an aluminum tube. The absorber material is positioned within the central thimble of the reactor by an experimental setup (such as the one described later in this paper). Two ECRDs are now available for experimental monitoring and controls research. The original 1991 ECRD (ECRD #1) is worth approximately 0.35$ and a recently constructed ECRD (ECRD #2) is worth approximately 0.94$. (The physical significance of reactivity, β, can be seen by its role in the physical process model that is summarized in the Appendix. The model is at equilibrium when reactivity is 0. A reactivity value equal to the delayed-neutron fraction, β, is referred to as 1$ of reactivity. If reactivity were suddenly changed from 0 to 1.1$, reactor power would initially increase exponentially with an undesirably fast period of about 0.045 seconds. If reactivity were suddenly changed from 0 to 0.5$, the initial asymptotic exponential period would be a more reasonable 5.5 seconds.) The control rods, which may only be positioned by the licensed control system, have reactivity that vary from about 3.0$ to about 5.0$. The maximum reactivity insertion rates with ECRD#1 and ECRD#2 are about 0.12$/s and 0.35$/s, respectively. ECRD #1 is used in experiments at power (up to 65%) where temperature changes produce significant reactivity feedback [10]. ECRD #2 was added in 2000 for use at low power (less than 0.1%) where temperature change and its reactivity feedback are negligible [11].

1.5 Experimental Computer Hardware and Software

A Pentium 550 MHz and an AMD 1000 MHz PC computer can be operated in two configurations for experiments that position an ECRD and thus control reactor power. A National Instruments data acquisition card is installed in the AMD computer. The AMD can be operated in a standalone mode where the graphical user interface and real-time application operate on the same computer using the Mathwork's MATLAB/SIMULINK real-time workshop windows real-time target option [12-14]. The second mode uses the MATLAB xPC real-time target option where a special real-time operating system is loaded on the AMD and it communicates with a windows-based graphical user interface on the Pentium computer.

2. ROBUST REACTOR CONTROL

To overcome the limitations found in classical control, robust control theory [e.g., 15-17] uses a *family* of models to represent the physical plant and characterize the uncertainty. This leads to a 'generalized' plant, which is then used to synthesize a 'robust' controller that guarantees both nominal performance and (robust) stability

when subject to uncertainty perturbations.

Uncertainty is the term for the differences between the physical system and the model, and it can be 'structured' or 'unstructured.' If the uncertainty perturbation is caused by a variation in a parameter associated with either the plant or the input, then the uncertainty perturbation is structured. If the uncertainty perturbation is dynamics-related, such as occurs when describing infinite-order or non-linear systems with a finite set of (linear differential) equations, then the uncertainty perturbation is unstructured. It is possible to model the parametric uncertainty as unstructured uncertainty, but this approach will be conservative [16]. The work reported here evaluates the approaches where 1) parametric uncertainty is handled separately, and 2) parametric uncertainty is covered by a larger unstructured uncertainty.

2.1 Linear Reactor models

Nonlinear point kinetics models of a reactor with two-temperature feedback (Appendix) are used to demonstrate and validate a variety of monitoring and control techniques for nuclear reactors [e.g., 2, 3, 4, 10, 11, 18, 19, 20]. The input signal u is velocity demand of the ECRD, R_{vd}. The measured output y is reactor power, n_r. A linear version of this model will vary as a function of equilibrium power level, n_{r0}, and responsiveness of the actual ECRD velocity to the input signal (velocity gain, R_{vg}). The robust control design objective for this problem is to obtain a low-order controller that can deal with a defined range of power levels and velocity gains. It is important to note that the model representing the TRIGA reactor is essentially a linearized model of the non-linear point kinetics with two-temperature feedback. This model does not capture the various non-linearities in the physical system, such as non-linearity in the ECRD actuation system from temperature and noise, noise in the instrumentation and control system, temperature effects on the reactor materials, and so on. This effort placed emphasis on examining the trade-off between handling model uncertainty and achieving acceptable performance, thus it sufficed to use a large linear TRIGA model. Future, and certainly non-trivial, effort could apply system identification techniques to capture the non-linear effects (e.g., temperature and noise) and thus more accurately characterize the uncertainty between the physical TRIGA and the reduced-order plant models derived in this work. Doing so would better illustrate the importance of minimizing dynamic uncertainty in order to maximize controller performance.

For the reactor application, the state vector comprises reactor power n_r, precursor density c_r (for one or six-delayed neutron group models), fuel temperature T_f, coolant temperature T_l, and ECRD position R_p. With six-delayed neutron groups, the model is 10th-order and is used as the basis to represent a family of plants. The linear 10th-order reactor model is:

$$\begin{bmatrix} \dot{\delta n}_r \\ \dot{\delta c}_{r1} \\ \dot{\delta c}_{r2} \\ \dot{\delta c}_{r3} \\ \dot{\delta c}_{r4} \\ \dot{\delta c}_{r5} \\ \dot{\delta c}_{r6} \\ \dot{\delta T}_f \\ \dot{\delta T}_l \\ \dot{\delta R}_p \end{bmatrix} = \begin{bmatrix} \frac{\beta}{\Lambda} & \frac{\beta_1}{\Lambda} & \frac{\beta_2}{\Lambda} & \frac{\beta_3}{\Lambda} & \frac{\beta_4}{\Lambda} & \frac{\beta_5}{\Lambda} & \frac{\beta_6}{\Lambda} & \frac{\alpha_f n_{r0}}{\Lambda} & \frac{\alpha_c n_{r0}}{\Lambda} & \frac{\alpha_r n_{r0}}{\Lambda} \\ \lambda_1 & -\lambda_1 & 0 & 0 & 0 & 0 & 0 & 0 & 0 & 0 \\ \lambda_2 & 0 & -\lambda_2 & 0 & 0 & 0 & 0 & 0 & 0 & 0 \\ \lambda_3 & 0 & 0 & -\lambda_3 & 0 & 0 & 0 & 0 & 0 & 0 \\ \lambda_4 & 0 & 0 & 0 & -\lambda_4 & 0 & 0 & 0 & 0 & 0 \\ \lambda_5 & 0 & 0 & 0 & 0 & -\lambda_5 & 0 & 0 & 0 & 0 \\ \lambda_6 & 0 & 0 & 0 & 0 & 0 & -\lambda_6 & 0 & 0 & 0 \\ \frac{f_f P_o}{\mu_f} & 0 & 0 & 0 & 0 & 0 & 0 & \frac{\Omega}{\mu_f} & \frac{\Omega}{\mu_f} & 0 \\ \frac{(1-f_f)P_o}{\mu_c} & 0 & 0 & 0 & 0 & 0 & 0 & \frac{\Omega}{\mu_c} & \frac{(M+\Omega)}{\mu_c} & 0 \\ 0 & 0 & 0 & 0 & 0 & 0 & 0 & 0 & 0 & 0 \end{bmatrix} \begin{bmatrix} \delta n_r \\ \delta c_{r1} \\ \delta c_{r2} \\ \delta c_{r3} \\ \delta c_{r4} \\ \delta c_{r5} \\ \delta c_{r6} \\ \delta T_f \\ \delta T_l \\ \delta R_p \end{bmatrix} + \begin{bmatrix} 0 \\ 0 \\ 0 \\ 0 \\ 0 \\ 0 \\ 0 \\ 0 \\ 0 \\ R_{vg} \end{bmatrix} \delta R_{vd} \quad (1)$$

$$y = [1\ 0\ 0\ 0\ 0\ 0\ 0\ 0\ 0\ 0] \begin{bmatrix} \delta n_r \\ \delta c_{r1} \\ \delta c_{r2} \\ \delta c_{r3} \\ \delta c_{r4} \\ \delta c_{r5} \\ \delta c_{r6} \\ \delta T_f \\ \delta T_l \\ \delta R_p \end{bmatrix} + [0]\ \delta R_{vd} \quad (2)$$

One of the two approaches for formulating a low-order nominal plant model, $P_o(s)$, for controller synthesis reported in this work starts with the above 10th order linear model and uses an optimal Hankel approximation to reduce the order to 4. The second approach for choosing $P_o(s)$ uses a one-delayed neutron group, which represents an average response of the delayed neutrons, and uses the singular-perturbation technique to eliminate the fast dynamics represented by the first state (referred to in nuclear engineering terminology as the one-delayed prompt-jump approximation). The resulting 4th-order linear model, based on this approximation of the "physics", is:

$$\begin{bmatrix} \dot{\delta c}_r \\ \dot{\delta T}_f \\ \dot{\delta T}_l \\ \dot{\delta R}_p \end{bmatrix} = \begin{bmatrix} 0 & \frac{\alpha_f \lambda n_{r0}}{\beta} & \frac{\alpha_c \lambda n_{r0}}{\beta} & \frac{\alpha_r \lambda n_{r0}}{\beta} \\ \frac{f_f P_o}{\mu_f} & \frac{\alpha_f f_f P_o n_{r0}}{\mu_f \beta} - \frac{\Omega}{\mu_f} & \frac{\alpha_c f_f P_o n_{r0}}{\mu_f \beta} + \frac{\Omega}{\mu_f} & \frac{\alpha_r f_f P_o n_{r0}}{\mu_f \beta} \\ \frac{(1-f_f)P_o}{\mu_c} & \frac{\alpha_f (1-f_f) P_o n_{r0}}{\mu_c \beta} + \frac{\Omega}{\mu_c} & \frac{\alpha_c (1-f_f) P_o n_{r0}}{\mu_c \beta} - \frac{(M+\Omega)}{\mu_c} & \frac{\alpha_r (1-f_f) P_o n_{r0}}{\mu_c \beta} \\ 0 & 0 & 0 & 0 \end{bmatrix} \begin{bmatrix} \delta c_r \\ \delta T_f \\ \delta T_l \\ \delta R_p \end{bmatrix} + \begin{bmatrix} 0 \\ 0 \\ 0 \\ R_{vg} \end{bmatrix} \delta R_{vd} \quad (3)$$

$$y = \begin{bmatrix} 1 & \frac{\alpha_f n_{r0}}{\beta} & \frac{\alpha_c n_{r0}}{\beta} & \frac{\alpha_r n_{r0}}{\beta} \end{bmatrix} \begin{bmatrix} \delta c_r \\ \delta T_f \\ \delta T_l \\ \delta R_p \end{bmatrix} + [0]\ \delta R_{vd} \quad (4)$$

2.2 Uncertainty specifications

As described earlier, Figure 3 presents a possible decomposition of the two dimensional operational space (reactor power, velocity gain), or (n_{r0}, R_{vg}), into nine operational regions (OR), where $0.45 < n_{r0} < 1.05$, and $0.25 < R_{vg} < 1.75$. With this framework, the system

uncertainty can be separated into parametric (structured) uncertainty and modeling (unstructured) uncertainty. From Figure 3, the variations in parametric uncertainty the process plant parameters n_{r0} and R_{vg} can be represented with additive uncertainty:

$$n_{r0} = n_{ij} + W_{nr}\,\delta_{nr} \tag{5}$$

$$R_{vg} = R_{ij} + W_{rvg}\,\delta_{rvg} \tag{6}$$

where n_{ij} is n_{r0} at the center of operating region OR_{ij}, R_{ij} is R_{vg} at the center of OR_{ij}, W_{nr} is the variation of n_{r0} within an OR, W_{rvg} is the variation in R_{vg} within an OR, and $\delta*$ represents an uncertainty perturbation whose magnitude is less than 1, but which can vary from –1 to 1.

The modeling uncertainty between a low-order model (at the center of an operating region) and a higher-order nominal model can be represented as input multiplicative uncertainty (uncertainty related to the actuator input to the reactor), and is represented by:

$$P_m(s) = P_o(s)(1 + \Delta_m(s)), \tag{7}$$

where

$$\Delta_m(s) = W_m(s)\,\delta_m(s) \tag{8}$$

with $W_m(s)$ being a frequency-dependent weighting function and δ_m representing an uncertainty perturbation.

Small modeling error and associated small multiplicative uncertainty is desirable to obtain robust controllers with better tracking performance. Figure 5 presents the magnitude plots of the transfer functions of both the tenth-order plant model and its one-group prompt-jump approximation. The main drawback to this approximation is the relatively large error at approximately $\omega = 0.2\ s^{-1}$ Figure 6 is the plot of the multiplicative uncertainty function (solid line) found by solving Equation (7) for $\Delta m(s)$. The multiplicative uncertainty at frequencies greater than $\omega = 10^2\ s^{-1}$ will be ignored for controller synthesis because the physical reactor plant cannot respond to inputs at the higher frequencies [1].

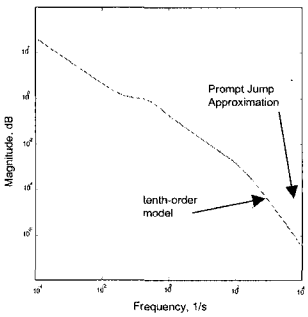

Fig. 5. Transfer Function of Tenth-order Reactor Plant and Prompt Jump Approximation.

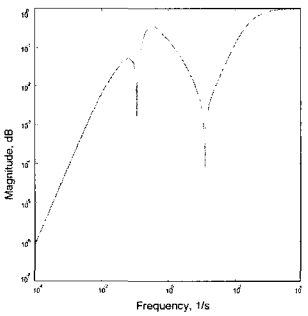

Fig.6. Modeling Uncertainty Between Tenth-order Reactor Plant and Prompt Jump Approximation.

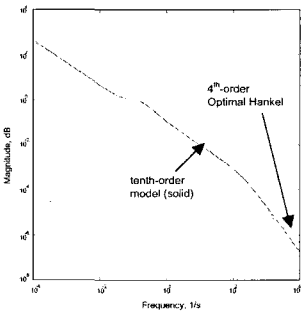

Fig.7. Modeling Uncertainty Between Tenth-order Reactor Plant and Prompt Jump Approximation.

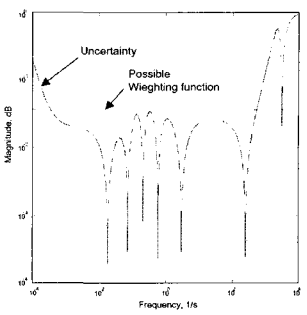

Fig.8. Modeling Uncertainty Between Tenth-order Reactor Plant and optimal Hankel approximation.

Figures 7 and 8 present transfer function magnitude and uncertainty-function plots where model-order reduction from 10 to 4 is accomplished via optimal Hankel reduction. A 4th order optimal Hankel approximation of the 10th order model is seen to be more accurate over a wider frequency range than is the one-group prompt-jump approximation, especially with significant reduction in the modeling error at $\omega = 0.2\ s^{-1}$.

However, the disadvantage of the optimal Hankel reduction, at this point in defining the problem for robust control design, is that the physical meaning of the states and state-space matrix elements is lost, and it is not clear how to incorporate the parametric uncertainty represented by Equations 5 and 6 on the parameters of the unreduced model. To overcome this problem, the approach used in this work uses the multiplicative uncertainty for a 4th–order optimal Hankel nominal plant model as formulated above but performs the model reduction after the parametric uncertainties have been manipulated into the framework required for robust control design, described in the following sections.

2.3 Performance Specifications

Another robust control specification is placed on nominal performance. Nominal performance is accomplished when the performance criteria are satisfied using the nominal plant [15-17]. The performance objectives could be that the plant output tracks the plant input with some minimal (tracking) error while minimizing control energy. Also, there could be design limitations on the effects of input and output plant disturbances, and design limitations on the effects of noise. For this work, the performance objectives were to minimize tracking error and control energy.

Figure 9 illustrates the initial orchestration of a nominal plant model (A,B,C,D), additive uncertainties due to Equations (5) and (6) (ΔA, ΔB), robust controller (K), multiplicative uncertainty (Δm), and, similarly, the performance specifications that will specify tracking

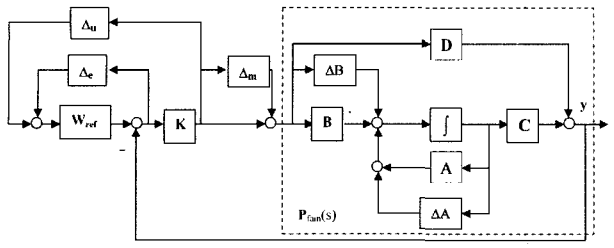

Fig. 9. Reactor Plant with Uncertainty and Performance Specifications.

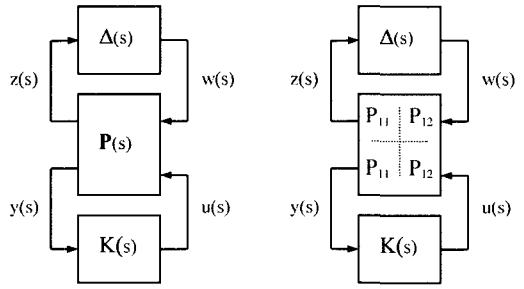

a) Representation for LFT b) with P(s) partitioned

Fig. 10. General Linear Fractional Transformation Representation.

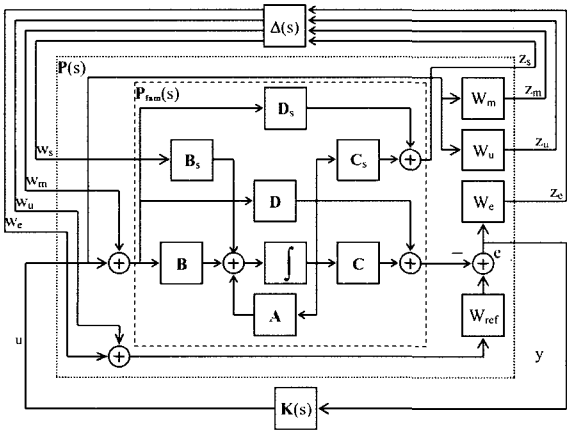

Fig. 11. LFT for the Reactor Control Application.

error and control energy performance requirements, respectively:

$$\Delta_e(s) = W_e(s)\,\delta_e(s) \tag{9}$$

$$\Delta_u(s) = W_u(s)\,\delta_u(s) \tag{10}$$

The representation of Figure 9 must be further manipulated and put into the framework required for controller (**K**) design using the μ-synthesis procedure [15-17] as shown in Figure 10. Figure 11 shows the necessary manipulation of Figure 9 to place the system into the framework of Figure 10 [21].

The dotted box of Figure 11 outlines the definition of **P**(s) needed in Figure 10 for robust control design, and $\Delta(s)$ is defined as: $\Delta(s) = \mathrm{diag}(\delta_e, \delta_u, \delta_m, \delta_s)$, with $\Delta_s = \mathrm{diag}(\delta_{nr}, \delta_{rvg})$. The matrices $\mathbf{B}_s$, $\mathbf{C}_s$, and $\mathbf{D}_s$, are selected to satisfy the following requirements:

$$\Delta\mathbf{A} = \mathbf{B}_s\,\Delta_s\mathbf{C}_s \tag{11}$$

$$\Delta\mathbf{B} = \mathbf{B}_s\,\Delta_s\mathbf{D}_s, \tag{12}$$

When working with the 4th-order one-delayed prompt-jump approximation model, **B**s, **C**s,

$$\mathbf{B}_S = \begin{bmatrix} \lambda W_{cr} & 0 \\ \dfrac{f_f P_o W_{cr}}{\mu_f} & 0 \\ \dfrac{(1-f_f)P_o W_{cr}}{\mu_c} & 0 \\ 0 & W_{Rvg} \end{bmatrix} \tag{13}$$

$$\mathbf{C}_S = \begin{bmatrix} 0 & \dfrac{\alpha_f}{\beta} & \dfrac{\alpha_c}{\beta} & \dfrac{\alpha_r}{\beta} \\ 0 & 0 & 0 & 0 \end{bmatrix} \tag{14}$$

$$\mathbf{D}_S = \begin{bmatrix} 0 \\ 1 \end{bmatrix} \tag{15}$$

and **D**s, are:

When working with the 10th-order nominal plant model, **B**s, **C**s, and **D**s, are:

$$\mathbf{B}_S = \begin{bmatrix} \dfrac{W_{nr}}{\Lambda} & 0 \\ 0 & 0 \\ 0 & 0 \\ 0 & 0 \\ 0 & 0 \\ 0 & 0 \\ 0 & 0 \\ 0 & 0 \\ 0 & 0 \\ 0 & W_{rvg} \end{bmatrix} \tag{16}$$

$$\mathbf{C}_S = \begin{bmatrix} 0 & 0 & 0 & 0 & 0 & 0 & 0 & \alpha_f & \alpha_c & \alpha_r \\ 0 & 0 & 0 & 0 & 0 & 0 & 0 & 0 & 0 & 0 \end{bmatrix} \tag{17}$$

$$\mathbf{D}_S = \begin{bmatrix} 0 \\ 1 \end{bmatrix} \tag{18}$$

Before proceeding to the μ-synthesis robust control design procedure [22-23], the 10th-order $P_{fam}(s)$, indicated within the dashed lines of Figure 9, is reduced to 4th order using the optimal Hankel Approximation. This procedure is thus the proposed method of using optimal Hankel reduction with parametric uncertainty specifications based on the parameters of the higher order model. This 4th-order optimal Hankel reduction procedure contrasts with the selection of a 4th-order model based on the physics of the one-delayed prompt-jump approximation, and a comparison of the results of the two approaches are presented in the next section.

3. RESULTS : SIMULATION AND VALIDATION

The parametric uncertainty (ΔA, ΔB) was studied to demonstrate the design trade-off between performance and uncertainty in the following forms: case 1) large enough that it covers a particular **OR**, case 2) large enough to cover the entire operating space, and case 3) no parametric uncertainty (all uncertainty handled as input multiplicative uncertainty).

The results of both computer simulation and experimental validation on the TRIGA reactor are presented. Experimental validation was carried out using the Mathwork's Real-Time Workshop tools [12-14]. Because TRIGA reactor operational guidelines placed a 55% limit on reactor power of 1 MW at the time of the experiments, the controllers were experimentally tested in OR_{13}, OR_{23}, and OR_{33}.

3.1 OR parametric uncertainty, Case 1

The parametric uncertainty covered only a particular OR. The ORs are equally sized, thus $W_{nr} = 0.10$ and $W_{rvg} = 0.25$ for all ORs. The nominal point will be the center of the OR for which the controller is being designed. For example, for OR_{11} the nominal point is $n_r = 0.95$ and $R_{vg} = 1.5$, or $p(0.95, 1.5)$, for OR_{33} it is $p(0.55, 1.5)$, etc.

It was found that the modeling uncertainty between the full-order reactor plant model and its optimal 4th-order Hankel approximation was significantly lower than that with the 4th-order one-group prompt-jump approximation. Hence, for the controllers derived using the optimal Hankel approximation, the input multiplicative uncertainty weighting functions could be set to constant values that did not vary appreciably ($0.033 \leq W_m \leq 0.036$) between ORs. The input multiplicative uncertainty weighting function for the one-delayed prompt-jump approximation derived controller in OR_{33} is:

$$W_m = 0.00007\left(\frac{\left(\frac{s}{0.0001}\right)+1}{s+0.25}\right) \qquad (19)$$

A search for the performance weighting functions W_e and W_u for each OR was required. The method involved setting loose initial specifications on control action while placing tighter restrictions, iteration by iteration, on steady-state error. When the time-domain non-linear simulation performance was deemed acceptable, iterations were then performed on control action until it was sufficiently minimized, again verified with a time-domain nonlinear simulation.

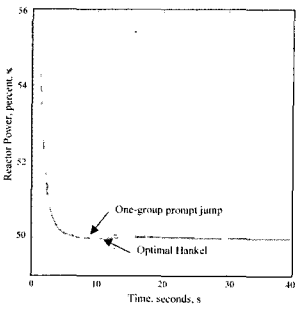

Fig.12. OR_{33}: 5% step change from $p(0.55,1.5)$.

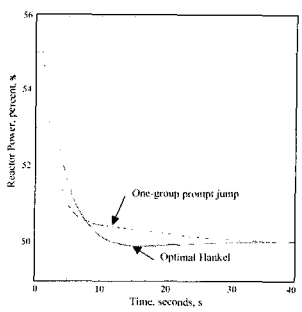

Fig.13. OR_{13}: 5% step change from $p(0.55,0.50)$.

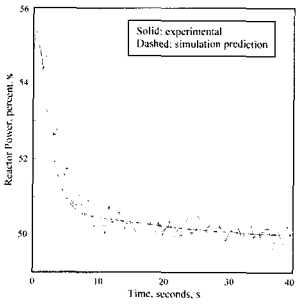

Fig.14. OR_{33}: 5% step change from $p(0.55,1.5)$.

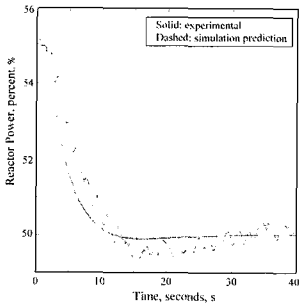

Fig.15. OR_{13}: 5% step change from $p(0.55,0.50)$.

Figures 12 and 13 show the simulation results within OR_{33} and OR_{13}, respectively. The input is a five percent step-down in the reactor power reference signal from either the nominal point $p(0.55, 1.5)$ for OR_{33} (Figure 12) or nominal point $p(0.55, 0.5)$ for OR_{13} (Figure 13).

At the high velocity gain, Figure 12, both controllers react similarly. However, at the low velocity gain, Figure 13, the optimal Hankel-approximation derived controller settles the system notably faster (with a small undershoot).

The experimental validation results are next presented in Figures 14 and 15 for the same step-down in reference signal from 55% reactor power and velocity gain of 0.5. Figure 14 is for the prompt-jump approximation-derived controller, and Figure 15 is for the optimal Hankel approximation-derived controller. The experimental one-delayed prompt-jump approximation-derived controller follows its simulation prediction very closely, and the experimental optimal Hankel-approximation derived controller has additional undershoot.

3.2 Large parametric uncertainty, Case 2

For this case, the parametric uncertainty covers the entire operating space of Figure 2. The nominal point is the center of the operating space, at which $n_{r0} = 0.75$ and $R_{vg0} = 1.0$, or $p(0.75,1.0)$. The parametric uncertainty weighting functions are thus: $W_{nr} = 0.30$, and $W_{rvg} = 0.75$. The input multiplicative weighting function for the one-group Prompt-jump Approximation for the nominal point $p(0.75,1.0)$ is

$$W_m = 0.000095\left(\frac{\left(\frac{s}{0.00018}\right)+1}{s+0.2}\right) \tag{20}$$

The input multiplicative uncertainty weighting function for the optimal Hankel approximation is set to a constant $W_m = 0.035$.

After finding suitable performance weighting functions, time domain performance of the controllers was assessed using nonlinear simulation. Figure 16 depicts the response of the one-group prompt-jump approximation-derived controller and the optimal Hankel approximation-derived controller to a five percent step-down in reference signal from 75% power with velocity gain of 1.5. Figure 17 presents the response to a five- percent step change reference signal from 55% reactor power with velocity gain of 0.5.

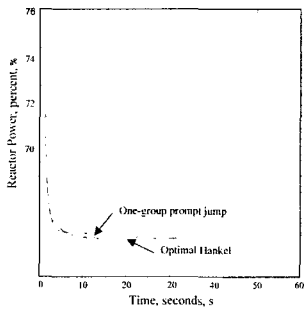

Fig.16. Entire operating space derived controllers $p(0.75,1.5)$.

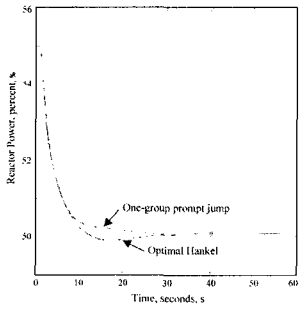

Fig.17. Entire operating space derived controllers $p(0.55,1.5)$.

Under these ideal simulation conditions it can be argued that the controller derived using the optimal Hankel approximation has the better performance as it has a marginally faster settling time than the controller derived using the one-group prompt-jump approximation. However, when evaluated on the TRIGA reactor, these differences could not be observed because of measurement noise [21].

3.3 No parametric uncertainty, Case 3

For this last case the parametric uncertainty is eliminated and the system uncertainty is covered only by input multiplicative uncertainty. The nominal point is the same as that for Case 2, specifically $p(0.75,1.0)$. By plotting the modeling uncertainty between the nominal point and each of the four extreme operating points (the four corners) of Figure 3—$p_1(0.45, 0.25)$, $p_2(0.45, 1.75)$, $p_3(1.05, 1.75)$, and $p_4(1.05, 0.25)$—the appropriate input multiplicative weighting function can be determined. For the one-group prompt-jump approximation, the required multiplicative uncertainty weighting function is:

$$W_m = 0.85\left(\frac{\frac{s}{0.1}+1}{\frac{s}{0.38}+1}\right) \tag{21}$$

For the optimal Hankel approximation, the required multiplicative uncertainty weighting function is

$$W_m = 0.85\left(\frac{\frac{s}{0.2}+1}{\frac{s}{0.38}+1}\right). \tag{22}$$

The experimental validation results for a five-percent step-down in reference signal from 55% power are given in Figures 18 and 19 for the one-group prompt-jump approximation derived controller and optimal Hankel-approximation derived controller, respectively. Even with measurement noise the advantage of the optimal Hankel approximation derived controller is apparent. Because all uncertainty is modeled as multiplicative, the settling time performance is also poorer than indicated in Figures 16 and 17 for Case 2 (additive and multiplicative uncertainty in a single operating space).

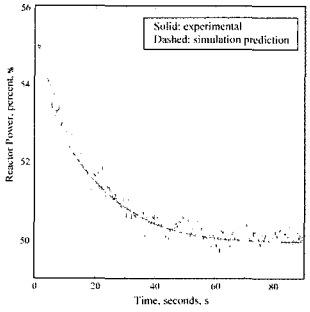

Fig.18. Multiplicative uncertainty only, prompt-jump approximation derived controller $p(0.55,1.5)$.

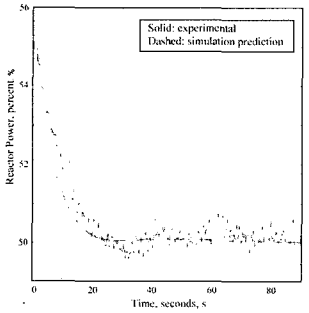

Fig.19. Multiplicative uncertainty only, optimal Hankel-approximation derived controller $p(0.55,1.5)$.

4. AN APPLICATION TO AUTONOMOUS SYSTEMS

Recall Figure 1 in Section 1.1, which depicts the hierarchical structure of a highly autonomous control architecture. The purpose of the supervisor level is to

select the proper controller based on the current operational mode (OM) and performance goals. The supervisor level is also the interface between the execution-level controllers and the coordination level. Not only is some type of system identification technique required, but also a controller switching scheme is required that does not cause step changes in the control action (bumpless transfer). Walter's work [1] successfully applied advanced system identification and intelligence-based switching algorithms during the development of a highly autonomous control system for the (shrouded) TRIGA. The scheme in this paper is not as ambitious as the intent is to demonstrate the performance of the μ-synthesized controllers in the high-autonomy framework, hence a simple supervisory level is developed.

One possible bumpless transfer scheme is that presented

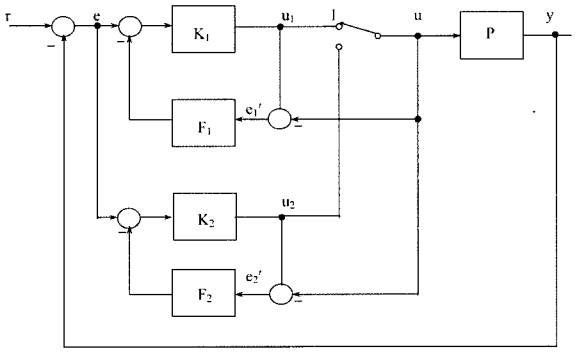

Fig. 20. Bumpless Transfer Scheme [17].

by Green and Limebeer in [17] (Figure 20). Assuming that initially the switch is in position 1, then controller K_1 is in closed-loop operation and controller K_2 is in open-loop operation. Also, let $|F_i| >> 1$ and $|K_iF_i| >> 1$. Thus, for K_1, $u = u_1 = K_1e$ and $e_1' \approx 0$, and, for K_2,

$$e_2' = (F_2)^{-1} e - (K_2F_2)^{-1} u_1 ,$$

and

$$u_2 = K_2e - K_2F_2e_2' = u_1 .$$

When the switch moves to position 2, the large value of F_1 quickly drives e_1' to (approximately) zero so that another bumpless transfer can be performed.

Instead of an intelligence-based switch-control scheme, a simple sequential logic circuit was developed (a 'state machine'), the decision variable inputs being reactor power, $n_r(t)$, and control action, u(t). The sequential logic circuit uses two J-K flip-flops, and the four states are:

00) $n_r(t) < 0.65$, $R_{vg} \geq 0.55$ fi in OR_{23} and K_{23} controlling
01) $n_r(t) < 0.65$, $R_{vg} < 0.55$ fi in OR_{13} and K_{13} controlling
10) $n_r(t) \geq 0.65$, $R_{vg} \geq 0.55$ fi in OR_{22} and K_{22} controlling
11) $n_r(t) \geq 0.65$, $R_{vg} < 0.55$ fi in OR_{12} and K_{12} controlling.

The relationship between rod velocity gain R_{vg} and control action, u(t), is found with a time-domain analysis using MATLAB's *Simulink* [12]. By inserting a fault condition on R_{vg}, the maximum allowable control effort in a particular OR was found. The four states can then be given in terms of the two decision inputs as such:

00) $n_r(t) < 0.65$, $|u(t)| < \max |u_{23}| = 11.18\%$fi in OR_{23} and K_{23} controlling
01) $n_r(t) < 0.65$, $|u(t)| < \max |u_{13}| = 11.65\%$ fi in OR_{13} and K_{13} controlling
10) $n_r(t) \geq 0.65$, $|u(t)| < \max |u_{22}| = 13.36\%$ fi in OR_{22} and K_{22} controlling
11) $n_r(t) \geq 0.65$, $|u(t)| < \max |u_{12}| = 17.43\%$ fi in OR_{12} and K_{12} controlling.

where max $|u^{**}|$ is the peak control action for controller K^{**} in OR^{**} that causes a state transition.

As the intention is only to demonstrate the switch control logic and the performance of the robust controllers in the framework of autonomous systems, only four states are necessary, and the state transitions *from* OM_1 to OM_2 are not considered. In order to include these state transitions, another decision variable will be required due to a hysteresis-like effect of control action. These state transitions represent the fault condition clearing itself, thereby simulating an intermittent rod actuator fault. However, even if all possible states and decision inputs were considered, the physical realization of the switch control logic circuit would not be too complex.

Three cases will be demonstrated: Case 1) transition from OR_{22} to OR_{23} (reactor power decreases from 67% to 62%); case 2) transition from OR_{22} to OR_{12} (faulted condition such that rod velocity gain decreases from nominal 1.0 to 0.5); case 3) transition from OR_{22} to OR_{23} to OR_{13} to OR_{12} (reactor power decreases from 67% to 62%, but a rod actuator fault occurs during the down-power transient, then an up-power transient from 62% to 67% power occurs). Finally, let controller K_{23} be 'controller 1', K_{13} be 'controller 2', K_{22} be 'controller 3', and K_{12} be 'controller 4'—these definitions are necessary to clarify the plots of the simulation results that follow.

Figure 21 shows the time-domain simulation results for Case 1, a down-power transient from 67% reactor

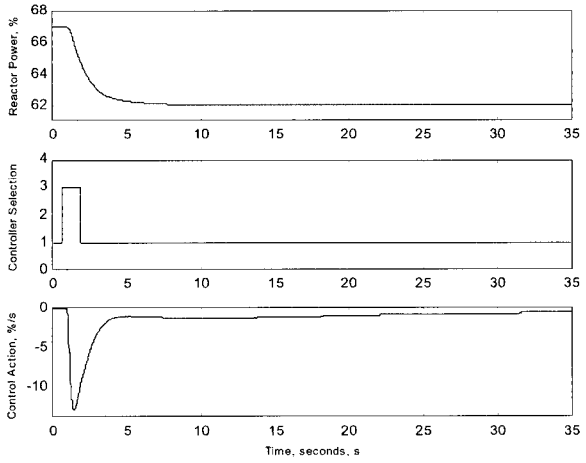

Fig. 21. Case 1. State Transition from OR22 to OR23.

power to 62% reactor power—OR_{22} to OR_{23}. The dashed line in the plot of reactor power represents the power level at which the state machine selects the proper controller. The state machine output is the plot labeled 'Controller Selection.' The down-power transient was initiated at t = 1.0 second, so the initial transition of the state machine logic from controller one to controller three was simply the state machine initializing itself. The units of control action in the bottom plot (labeled 'Control Action') are percent rod length per second, and there is no adverse effect on control action due to the switching of controllers during the transient.

Case 2 was a rod actuator fault during a down-power transient from 75% reactor power to 70% reactor power. The fault is a step-change in rod velocity gain, Rvg, from 1.0 to 0.5, so a transition from controller K_{22} (3) to controller K_{12} (4) occurs. The fault is initiated at the beginning of the transient, t = 1.1 seconds. The simulation results are given in Figure 22, but the top figure is now

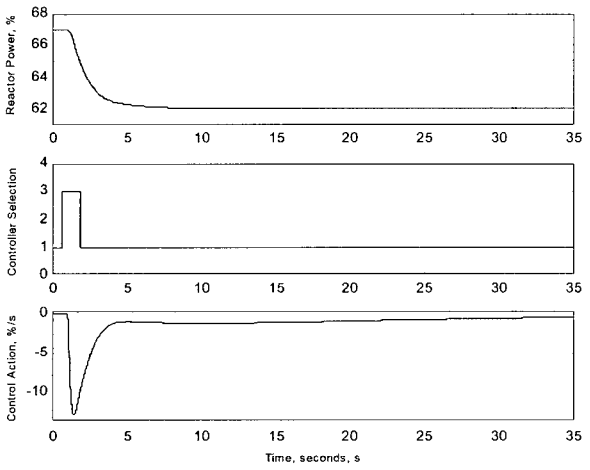

Fig. 22. Case 2. State Transition from OR22 to OR12.

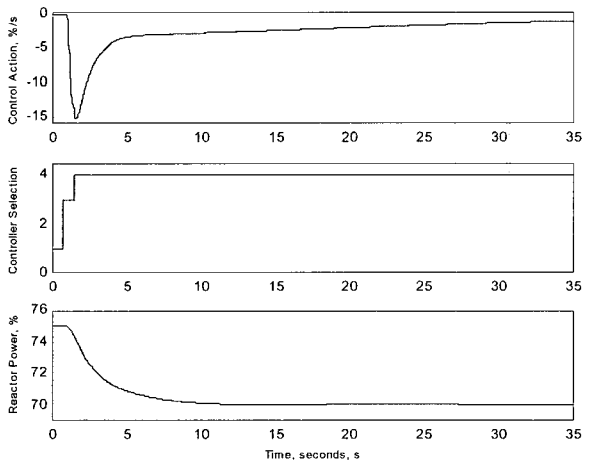

Fig. 22. Case 2. State Transition from OR22 to OR12.

control action (the dashed line is the trip level). The initial transition of the state machine logic (from 1 to 3) in the plot of Controller Selection is again the initialization of the state machine.

These two cases taken independently only serve to demonstrate the state machine implementation. Further, Case 2 is simplistic in that the fault is conveniently initiated at the beginning of the transient. Case 3 combines elements of the previous cases and adds one in that the fault is initiated near the end of a down-power transient —see Figure 23.

Initially, controller K_{22} (3) is controlling the system. At t = 1.0 second, a down-power is initiated from 67% reactor power (top plot) down to 62% reactor power, and control is transferred to controller K_{23}. The rod actuator fault—a step-change in rod velocity gain from 1.0 to 0.5—occurs at t = 10.0 seconds. At t = 10.0 seconds, the tracking error is significantly reduced, though still not zero, thus additional reactivity must be inserted into the system to achieve a zero steady state error. Since the rate of reactivity insertion is significantly reduced, reactor power begins to rise and the controller must expend more energy to reduce the tracking error to zero. Because the fault occurred late in the transient, control energy (bottom plot) does not reach the trip point of –11.18 percent rod length per second.

An up-power transient is initiated from near steady state at t = 35.0 seconds. This time the state machine switch logic determines that a rod actuator fault exists and switches to controller K_{13} (2). Soon after the switch, reactor power exceeds 65% and the state machine selects controller K_{12} (4) to finish the transient. See [1] for a more advanced implementation of a bumpless transfer scheme in which fuzzy logic and on-line performance monitoring are utilized.

5. CONCLUSION

A robust control design procedure for a nuclear reactor has been developed and experimentally validated on the Penn State TRIGA research reactor. The optimal Hankel approximation and a combination of additive and multiplicative uncertainty are the best approach to design robust control for this application. The results from nonlinear simulation testing and the physical experiments are consistent and thus help to confirm the correctness of the robust control design procedures and conclusions.

Finally, the robust controllers developed in this work were applied to an autonomous control system with the use of a simple state-machine-based switch controller that provided bumpless transfer initiated by specific combinations of two decision variables.

APPENDIX, Nonlinear reactor kinetics incorporating two-temperature feedback and Experimental Changeable Reactivity Device velocity demand (R_{vd}) as the control

input and relative reactor power (n_r) as the plant output:

$$\frac{dn_r}{dt} = \frac{\rho(t)-\beta}{\Lambda} n_r + \sum_{i=1}^{G} \frac{\beta_i}{\Lambda} c_{ri} + q_r \qquad \text{(A-1)}$$

$$\frac{dc_{ri}}{dt} = \lambda_i n_r - \lambda_i c_{ri}, \quad i=1,2,\ldots G \qquad \text{(A-2)}$$

$$\frac{dT_f}{dt} = \frac{f_f P_0}{\mu_f} n_r - \frac{\Omega}{\mu_f}(T_f - T_c) \qquad \text{(A-3)}$$

$$\frac{dT_l}{dt} = \frac{(1-f_f)P_0}{\mu_c} n_r + \frac{\Omega}{\mu_c}(T_f - T_c) - \frac{M}{\mu_c}(T_l - T_e) \qquad \text{(A-4)}$$

$$\frac{dR_p}{dt} = R_{vg} R_{vd} \qquad \text{(A-5)}$$

$$\rho(t) = \alpha_r\left(R_p(t) - R_{p0}\right) + \alpha_f\left(T_f(t) - T_{f0}\right) + \alpha_c\left(T_c(t) - T_{c0}\right) \qquad \text{(A-6)}$$

$$T_c(t) = wT_l(t) + (1-w)T_e(t) \qquad \text{(A-7)}$$

where

- n_r ≡ n/n_{100} neutron density relative to full-power equilibrium density,
- c_{ri} ≡ c_i/c_{i00} density of delayed-neutron precursor group i relative to group i full-power equilibrium density,
- n ≡ neutron density, neutrons per cm^3",
- c ≡ density of delayed neutron precursor group i, atoms per cm^3,
- n_{100} ≡ full-power equilibrium neutron density,
- c_{i00} ≡ full power equilibrium delayed-neutron precursor group i density,
- q_r ≡ q/n_{100} external neutron source relative to full-power equilibrium neutron density,
- q ≡ external neutron source , neutrons per cm^3/sec",
- G ≡ number of delayed neutron groups,
- λ_i ≡ radioactive decay constant (1/s) of precursor group i,
- Λ ≡ effective prompt neutron lifetime in seconds,
- β_i ≡ fraction of fission neutrons which come from delayed group i,=1....G
- $\beta = \sum_{i=1}^{G} \beta_i$ ≡ total delayed neutron fraction,
- $\rho = \frac{k-1}{k}$ ≡ reactivity. Note that at equilibrium (k=1), ρ=0.
- k ≡ keff ≡ effective neutron multiplication factor,
- T_f ≡ Average fuel temperature in ℃
- T_l ≡ Temperature of the coolant leaving the reactor in °C
- T_e ≡ Temperature of the coolant entering the reactor in °C
- T_c ≡ Average coolant temperature in °C
- w ≡ weighting factor on Tl for computation of Tc
- P_0 ≡ rated reactor power, MW.
- f_f ≡ fraction of power deposited in the fuel
- μ_f ≡ Product of fuel mass times heat capacity, MW-s//°C
- μ_c ≡ Product of coolant- channel mass times heat capacity, MW-s//℃
- M ≡ Product of coolant flow rate times heat capacity, MW/℃
- Ω ≡ heat transfer coefficient between fuel and coolant, MW/℃
- R_P ≡ position of Experimental Changeable Reactivity Device (ECRD), fraction withdrawn from the reactor.
- R_{vg} ≡ velocity gain of the ECRD.
- R_{vd} ≡ ECRD velocity demand signal
- α_r ≡ reactivity due to change in R_p
- α_f ≡ reactivity due to change in T_f
- α_c ≡ reactivity due to change in T_c
- R_{p0} ≡ R_p at time 0.
- T_{f0} ≡ T_f at time 0.
- T_{c0} ≡ T_c at time 0.

Table of TRIGA Reactor Model Parameters:

α_f = -0.00014 (Δk/k per ℃)	P_0= 1 MW	β = 0.0069949	λ =0.1 s^{-1} (G=1)
α_c = 1e-08 (Δk/k per °C)	Λ = 0.000038 s	β_1 = 0.000231	λ_1= 0.000231 s^{-1}
α_r = 0.35β =0.002448 Δk/k	w =1.0	β_2 = 0.001528	λ_2 = 0.03051 s^{-1}
μ_f = 0.103 MW-s/ °C	f_f = 0.99	β_3 = 0.001372	λ_3 = 0.114 s-1
μ_c = 0.072 MW-s/ ℃	$T_e(t)$ = 20 ℃	β_4 = 0.002765	λ_4 = 0.3013 s-1
M(t) = 0.05 MW/ ℃	$q_r(t)$ = 0	β_5 = 0.0008049	λ_5 = 1.1362 s-1
Ω = 0.0056 MW/ ℃		β_6 = 0.000294	λ_6 = 3.0135 s-1

REFERENCES

[1] Walter, Phillip B., "Development of an Intelligent Control System with a High Degree of Autonomy and Application to Nuclear Power Systems," Doctor of Philosophy paper in Nuclear Engineering, The Pennsylvania State University (May 1997).

[2] Edwards, R.M., K.Y. Lee and D.E. Hughes, "Testbed For Nuclear Plant Instrumentation And Control Validation," *Proceedings of The 1996 American Nuclear Society International Topical Meeting on Nuclear Plant Instrumentation, Control and Human Machine Interface Technologies, NPIC&HMIT '96*, pp. 287-294, University Park, PA, (May 6-9, 1996).

[3] Edwards, R.M. "Integration of a Thermal-Hydraulic Test-loop and University Research Reactor for Advanced Monitoring and Control Research," *Proceedings of The Third American Nuclear Society International Topical Meeting on Nuclear Plant Instrumentation, Control and Human-Machine Interface Technologies, NPIC&HMIT '2000*, 8 pages (on CD ROM), Washington, DC (November 12-16, 2000).

[4] Edwards, Robert M., S.J. Kenney and K.Y. Lee, *Experimental Development of Power Reactor Intelligent Control Final Report*, EPRI TR-109181, vol. 1-4 (November 1997).

[5] Edwards, R. M., K. Y. Lee and M. A. Schultz, "State Feedback Assisted Classical Control: An Incremental Approach to Control Modernization of Existing and Future Nuclear Reactors and Power Plants," *Nuclear Technology*, Vol. 92, pp. 167-183, November 1990.

[6] Edwards, R. M., K. Y. Lee and A. Ray, "Robust Fault-Accommodating Control of Nuclear Reactors and Power Plants," *Nuclear Technology*, Vol. 98, pp. 137-148, May 1992.

[7] Ramaswamy, P., R. M. Edwards, and K. Y. Lee, "An Automatic Tuning Method of a Fuzzy Logic Controller for Nuclear Reactors," *IEEE Transactions on Nuclear Science*, Vol. 40, No. 4, pp. 1253-1262, August 1993.

[8] Ku, C.-C., K. Y. Lee and R. M. Edwards, "Improved Nuclear Reactor Temperature Control Using Diagonal Recurrent Neural Networks," *IEEE Transactions on Nuclear Science*, Vol. 39, No. 6, pp. 2298-2309, December 1992.

[9] Hughes, D.E., Mac Bryan, and Robert Gould, "Safety Issues Involved in Using the PSBR for Control Algorithm Testing," *Proceedings of AI 91: Frontiers in Innovative Computing for the Nuclear Industry*, Jackson Wyoming (Sept 15-17,1991).

[10] Shaffer, R., W. He, and R.M. Edwards. 2004. Design And Validation Of Optimized Feedforward With Robust Feedback Control Of A Nuclear Reactor. *Nuclear Technology*, 147: 240-257

[11] Huang, Z., and R.M. Edwards. 2003. Hybrid Reactor Simulation of BWR Power Oscillations. *Nuclear Technology*. 143:132-143.

[12] *SIMULINK, Dynamic System Simulation Language User's Guide*, The Mathworks, Inc. (1994).

[13] *Real-Time Workshop User's Guide*, The Mathworks, Inc. (1999).

[14] *Real-Time Windows Target User's Guide*, The Mathworks, Inc. (1999).

[15] Pena, R.S. Sanchez and M. Sznaier, Robust Systems Theory and Applications, Preprint (1998).

[16] Zhou, K. and J.C. Doyle, *Essentials of Robust Control*, International Ed., Prentice-Hall, Inc. (1998).

[17] Green, M. and D.J. *Limebeer, Linear Robust Control*, International Ed., Prentice-Hall, Inc. (1995).

[18] Edwards, R.M., K.Y. Lee and Asok Ray, 1992. Robust Optimal Control of Nuclear Reactors and Power Plants, *Nuclear Technology*, 98:137-148.

[19] Ceceñas-Falcón, M., and R.M. Edwards. 2003. Out-of-Phase BWR Stability Monitoring. *Nuclear Technology*. 143: 125-131.

[20] Shyu, S., and R.M. Edwards. 2002. A Robust Multivariable Feedforward/Feedback Controller Design for an Integrated Power Control of Boiling Water Reactor Power Plants. *Nuclear Technology*. 140:129-146.

[21] Shaffer, Roman A., "Design, Simulation, and Validation of Robust Controllers," Master of Science paper in Nuclear Engineering, The Pennsylvania State University (May 2000).

[22] Chiang, R.Y. and M.G. Safonov, *Robust Control Toolbox*, The Mathworks, Inc. (1992).

[23] Balas, G.J., J.C. Doyle, K. Glover, A. Packard, and R. Smith, *μ-synthesis and Analysis Toolbox*, The Mathworks, Inc. (1995).